AGARD-CP-567

AGARD

ADVISORY GROUP FOR AEROSPACE RESEARCH & DEVELOPMENT
7 RUE ANCELLE, 92200 NEUILLY-SUR-SEINE, FRANCE

AGARD CONFERENCE PROCEEDINGS 567

Propagation Assessment in Coastal Environments

(l'Évaluation de la propagation en régions côtières)

Papers presented at the Sensor and Propagation Panel Symposium, held in Bremerhaven, Germany 19-22 September 1994.

NORTH ATLANTIC TREATY ORGANIZATION

Published February 1995

Distribution and Availability on Back Cover

LIDAR MEASUREMENTS OF REFRACTIVE PROPAGATION EFFECTS

C. R. Philbrick and D. W. Blood
Applied Research Laboratory/Penn State University
P.O. Box 30, State College, PA 16804 USA
(814) 863-7682 - FAX (814) 863-8783

1. SUMMARY

A multi-wavelength Raman lidar has been developed and used to measure the profiles of atmospheric properties in the troposphere under a wide range of geophysical conditions. The instrument measures the two physical properties which contribute to the refractive index at radio frequencies, water vapor concentration profiles from vibrational Raman measurements and neutral density determined from rotational Raman temperature profiles and surface pressure. The LAMP lidar instrument is transportable and has been used to make measurements at several locations in addition to our local Penn State University site, including shipboard measurements between Arctic and Antarctic and in the coastal environment at Point Mugu, CA. Lidar measurements of the atmospheric refractive environment, which are of particular interest, were made during 1993 at Point Mugu, CA, including the period of Project VOCAR (Variability of Coastal Atmospheric Refractivity). Both the lidar and balloon tropospheric measurements have been used for analyses of the propagation conditions by employing the Navy's RPO, IREPS and EREPS PC programs and comparisons have been made with the measured propagation conditions. On the short term (hour-to-hour throughout a day), the lidar derived profiles permit the examination of refractive layer stratification for guided-wave mode propagation.

2. INTRODUCTION

During the VOCAR program of 1993, lidar measurements of the coastal atmospheric profiles of water vapor and temperature were made at Point Mugu, CA (see description of the VOCAR program, Ref 1). One of the primary purposes was to produce refractivity profiles of the lower troposphere during variable coastal atmospheric conditions to verify that lidar measurements, as well as balloon/radiosonde measurements of the atmospheric refractivity could be used as input to propagation models for evaluation of the propagation effects which are known to range from normal atmospheric propagation to highly ducted radiowave propagation in this ocean and coastal region. A useful overview of the RF propagation characteristics and models for the lower atmosphere is available (Ref 2) and the particular propagation characteristics of the coastal environment have been discussed in this volume (Ref 3).

Penn State University/Applied Research Laboratory was invited to participate in the VOCAR program, which involved a wide variety of meteorological sensors coordinated for the purpose of characterizing the spatial and temporal variability of the refractive environment at sea, and along the California coastline. The portable research instrument, referred to as the PSU/LAMP lidar (Ref 4), was placed strategically at the Point Mugu NAWC during the 1993 program, near the Geophysics Division, where the weather station is located and where frequent balloon launchings of radiosondes were carried out during the intensive data collection periods.

The LAMP lidar transmitter uses a Nd:YAG laser which has an output of 1.5 j at 20 Hz at the 1064 nm fundamental output. The beam is passed through a doubling crystal and a mixing crystal to produce the 532 and 355 nm, or 266 nm, beams which are used for the lidar measurements. The primary receiver is a 42 cm diameter Cassegrain telescope. The low altitude backscatter signals of the visible and ultraviolet beams can be detected as analog signals and digitized at 10 MSps to provide 15 meter resolution from the surface to 25 km, or detected as photon count signals with 75 m altitude resolution. The high altitude signals, obtained by photon counting techniques, are accumulated into 500 nanosecond range bins to provide 75 meter resolution, from 20 to 80 km. The high altitude detector also contains low altitude photon counting channels which measure the first Stokes vibrational Raman signals of the N_2 and the H_2O Raman scatter. The low altitude detector has eight channels to measure the backscatter signal at two laser fundamental lines, two N_2 Raman lines, two H_2O water vapor lines and two segments of the rotational Raman envelope. The transmitter, receiver, detector, and data system combination have been integrated into a standard shipping container, which serves as a field laboratory.

A recent review (Ref 5) of the vibrational and rotational Raman scattering techniques has clearly shown that these approaches have the capability of measuring the minor species and structure properties, as well as the optical properties, of the lower atmosphere, even in the presence of a small amount of interference from the background aerosol environment. The Raman technique measures the profiles of water vapor from the ratio of Raman vibrational backscatter signals of water vapor to those of nitrogen. The lidar has been used to obtain water vapor profiles from molecular Raman vibrational scattering at several wavelengths and temperature profiles from Raman rotational scattering at 528 and 530 nm. The water vapor measurements have been made using the vibrational Raman backscatter intensity from the 660/607 ratio from the 532 nm, 407/387 ratio from 355 nm, or the 294/283 ratio from 266 nm laser radiation. Having two sets of measurements allows additional examination of the small scale structure and the wavelength dependence of the correction for aerosol differential extinction. The quadruple (266 nm) Raman scatter signals have been examined and used for daytime measurements where the troposphere is shielded from wavelengths below 300 nm (solar blind region) by the stratospheric ozone absorption. These ultraviolet measurements are slightly complicated by the need to make corrections for the absorption of tropospheric ozone.

The profiles of water vapor and temperature, and ground based pressure data, were averaged and used to compute profiles of refractivity, N and modified refractivity, M, at 75 m resolution in the lower tropospheric region (0-5000 m). The lidar data is stored at one minute intervals and the temporal variation of refractive index is typically examined at intervals of 30 minutes. The profiles are analyzed for refractive layer structures which influence electromagnetic wave propagation over the ocean and near-coastal regions. Under summer atmospheric conditions, periods of persistent surface-based ducting (trapping layers) of horizontally propagating radio waves are frequently observed. The effects of ducts over the ocean path environments were sensed by measured signal levels on several ocean and coastal radio paths monitored by NCCOSC/NRaD at VHF and UHF bands during the measurement campaign (Ref 6).

3. PROPAGATION EFFECTS IN A COASTAL ENVIRONMENT

For the entire VOCAR period, NCCOSC/NRaD established and operated a radio path signal monitoring network of several VHF and UHF transmission source signals at both Point Mugu and San Diego, CA (Ref 6). The multiple source signals were sampled,

Paper presented at the Sensor and Propagation Panel Symposium on "Propagation Assessment in Coastal Environments" held in Bremerhaven, Germany 19-22 September 1994.

through the use of a programmable spectrum analyzer, and processed for a continuous synoptic monitoring of the received signal level every 15 minutes. Available ATIS (Automatic Terminal Information System) transmissions from both commercial and military airports were monitored and recorded. In addition, separate VHF and UHF continuous wave transmissions dedicated to the VOCAR program, were installed at San Clemente Island, and monitored at the two reception points on a routine basis. These two path lengths were nearly identical, however with different ocean path directions. The San Clemente Island-to-Point Mugu path distance is 132 km.

Figures 1 and 2 show a seven day segment of both the San Clemente Island (SCI) UHF (374.95 MHz), and VHF (143.09 MHz) received signal level histories at Point Mugu, CA, during the VOCAR intensive data collection period of August 1993. PSU Lidar operations were conducted on a daily basis during each night-to-daytime period of the VOCAR program. The five such operational periods (which will be discussed further) are highlighted in the figures. It is observed that the signal levels varied over a 40-50 dB range during the period from August 25 to September 1. The sequence of days analyzed illustrate the major changes in near-surface propagation and refractive effects that occurred during VOCAR. The five lidar operation day periods analyzed were in a period with major changes in the atmospheric conditions. These ranged from days with greatly enhanced propagation to days with standard propagation and losses beyond the horizon. During periods of surface refractive ducting (so-called anomalous) conditions the beyond-line-of-sight paths exhibited very strong signal levels reaching and exceeding that of free space propagation. Under standard refractive conditions, low signal strengths were received as would be predicted during non-ducting tropospheric conditions.

4. LIDAR MEASUREMENTS OF REFRACTIVITY

The primary measurements by lidar for this study consisted of water vapor and temperature profiles obtained by Raman (vibrational and rotational) line ratio spectral measurement techniques discussed. Examples of the lidar-measured parameters are shown in Figures 3 and 4 respectively, starting at 1013 UT on the 26th of August 1993. The photon counts were accumulated in 75 meter range/altitude bins and over one minute intervals. The profiles shown, however consist of 30 such interval accumulations combined, and therefore represent a 30 minute averaged period. The statistical error bars (+/- standard deviation) are shown on the solid lines for the lidar measurements. The near time balloon (radiosonde profile) measurements, expressed in the same units (g/kg) for water vapor and (degree K) for temperature, are shown as dashed lines in the figures for comparison with the lidar measurements. The balloon and lidar atmospheric measurements, although agreeing very well in general, often times show slight departures in measured profile details attributable to the different temporal and spatial sampling of the drifting balloon versus the perfectly vertical (single location) profile of the lidar. The measured temperature and water vapor, together with an atmospheric pressure value derived from an integration of the hydrostatic equation using the lidar measurements, constitute the inputs to the standard and accepted equation for refractivity. Although measured by lidar to above 5000 m altitudes, only the lower tropospheric region profile from the surface to 1500 m is presented in this analysis to describe the refractive conditions for near-surface propagation.

The computed refractivity (N) and modified refractivity (M) profiles, corresponding to the water vapor and temperature data of Figures 3 and 4, are shown in Figure 5. On 26 August 1993, the rapid decrease in water vapor combined with the temperature inversion (positive lapse rate) produced gradients in refractivity sufficient for the trapping of horizontally propagating electromagnetic waves. The strong ducting conditions start very near the surface and the duct height extends to nearly 600 m above the surface. Figure 5 at 1013 UT is just one of the entire sequence of 30 minute accumulated profiles taken throughout the lidar operation period on this date. The entire series of M-profiles on 26 August is portrayed in the Figure 6 three dimensional surface plot of modified refractivity versus altitude and time.

Similar conditions existed on 27 August, Figures 7 and 8, except that the surface based duct height is lower, extending only to 350 m instead of 600 m. Referring back to Figures 1 and 2, the enhanced received signal levels are comparable on the two days. On 28 August, the ducting condition tends to lift from the surface with a surface based elevated duct to heights of 425 m, as evident in Figures 9 and 10. The corresponding signal levels drop by at least 10 dB on this date. Surface-based ducting has ceased by August 29th , and the Figures 11 and 12 show only an elevated duct conditions remains in the altitude region of 350 to 500 m in the time period of 0800 UT. Once more, the signal levels as indicated in Figures 1 and 2 have dropped further by about 10 dB from the previous day.

Finally, by 31 August, evidence of even an elevated duct is gone, and the profile data of Figure 13 shows a lack of any elevated duct. The time history is shown in Figure 14 with a long sequence of stable refractive conditions and little variability. The signal levels have now reached the lowest levels of up to 40 dB below the strongly enhanced conditions of 26 August when ducting near the surface occurred.

5. RESULTS OF PROPAGATION MODELING USING LIDAR PROFILES

The propagation conditions may be analyzed in more detail by using the Navy's RF propagation modeling programs such as IREPS, EREPS and RPO (Refs 7, 8, and 9), which have been incorporated into PC applications. The lidar profiles have been prepared as input to these programs, originally designed for radiosonde input and for refractive effects assessment. The five days and two frequencies constitute a set of 10 measurement-days which have been analyzed to evaluate the qualitative aspects of the changing refractive effects and the propagation loss characteristics that would have been predicted, given the lidar profile data as an input.

Table 1 shows the predicted propagation loss as would have been obtained by IREPS, the first propagation analysis tool developed (Ref 7), and by the recent RPO (Radio Physical Optics) program provided by NCCOSC/NRaD (Ref 9). The 132 km San Clemente Island to Pt. Mugu over ocean path is analyzed for comparison by the two programs. The early IREPS software only crudely analyzes the propagation losses, and inadequately solves for the field for long beyond-the-horizon distances (loss relative to free space, 5th column of Table 1). The RPO program, however, provides a more precise measure of the propagation losses by computing the field strength at any range and elevation from a source transmission, given refractive profiles as input which are representative of the path conditions. Although RPO will accept a range-dependent set of refractivity profiles, the profiles from the Point Mugu lidar are input as a single profile representative of the path, although measured and obtained at the path endpoint only. Further, the lidar profiles shown in Figures 5, 7, 9, 11, and 13 have been piece-wise smoothed (linear) to simplify the data entry into RPO and IREPS. The latter is not a requirement for RPO, however. The RPO predicted losses relative to free space and the total path losses are given in the 6th and 7th columns respectively. Note that the total path losses from 8/26 to 8/31 span a 40 dB range of differences.

The coverage and loss plots of RPO are instructive in terms of understanding where physically the signals propagate and what waveguide modal effects contribute to a signal enhancement or to

an excessive loss over the propagation path. Figure 15 shows the propagation loss contour output of RPO for the UHF frequency (374.95 MHz) on 8/26. The contours are for 2.5 dB steps of increasing loss on a height versus range display. During surface-based ducting, the EM wave propagates within the duct to great ranges beyond the curvature of the earth. Figure 16 shows the loss versus height at the fixed range corresponding to the receiver distance from the source transmitter (132 km in this case). Notice that enhancements or deficits in signal can occur very rapidly with receiving antenna height change. The receiving antenna at Pt. Mugu in this case is at 30.5 m, very near the bottom portion of the curve. Figure 17 shows the loss as a function of range with a constant height antenna at 30.5 m, that used for VOCAR. Figures 18, 19 and 20 represent the same plots showing the VHF signal level (143.09 MHz) variations predicted for 8/26. Notice that at this frequency, the free space losses are not reached even though the ducted signals are enhanced above that for standard refractive profile environments.

Table 2 also shows the RPO computed losses but compares them with the observed losses at UHF and VHF (column 4) from Figures 1 and 2. The VOCAR signal path losses have been scaled from the signal level data of Figures 1 and 2 with approximate levels and extremes within +/- 3 hours of the specific lidar collection date interval using the available 15 minute sampled signal level data. The RPO predictions (using lidar data profiles as input) are shown in column 5 in dB relative to free space. The differences between the scaled observed signal and the predicted RPO level are shown in column 6. On individual dates and times the RPO prediction using a single profile and a relatively approximate scaling of data, the path losses can only be estimated to with about +/- 10 dB. Overall, however the average of the ten frequency measurement-day differences which were either too high or to low is less than one dB.

The lidar atmospheric sensor has proven to provide good temporal and vertical sampling of refractive variability. The path-integrated signal level variability, however, depends upon the horizontal homogeneity of the refractivity profile. The spatial homogeneity or variability of refractive index has been examined further during VOCAR by multiple sensors, aircraft flights, and other techniques (Ref 10). The widespread characterization of refractive ducting through changing weather fronts has been explored through the use of GOES satellite imagery (Ref 11).

One can conclude that on the whole, the propagation predictions based on a single lidar profile are useful to provide first order estimates of the losses that can occur on a propagation path. This has been applied to time periods when persistent refractive conditions have occurred, indicative of widespread stability. An arbitrary refractive profile is obtained to represent the prevailing conditions, and horizontal homogeneity is assumed over the path. Further analysis will be required to determine if improvement below +/-10 dB case-by-case level can be achieved with a more detailed time history of the lidar and signal level data sets. The general features of widely varying day-to-day signal levels are predicted in accordance with the observed signal levels with conditions ranging from strong surface-based ducting to the absence of ducting in the lower tropospheric refractive profile.

6. ACKNOWLEDGEMENTS

Special appreciation for the support and encouragement of this work goes to Dr. Juergen Richter, CDR. Dave Markham and CDR. Pete Ranelli. The opportunity to directly compare the lidar derived refractivity to the measurements of electromagnetic wave ducting was made possible by efforts of H. Hitney, R. Paulus and T. Rogers of NCCOSC NRaD. J. Rosenthal, J. Borgen and R. Helvey of the meteorological office of Geophysics Division, Safety Officer G. Wadley of the Naval Air Warfare Center at Point Mugu, CA, and W. Lee of SPAWAR contributed much to the success of the project. The efforts of D. B. Lysak, Jr., R. E. Erdley, T. J. Kane, J. Jenness, T. Petach, T. D. Stevens, P. A. T. Haris, Y.-C. Rau, S. Rajan, B. Mathason, M. O'Brien, S. C. McKinley, S. Maruvada, G. Evanisko, G. Pancoast, W. W. Moyer and E. Harpster have contributed much to the success of this project.

7. REFERENCES

1. Paulus, R.A., "An overview of an intensive observation period on Variability of Coastal Atmospheric Refractivity," NCCOSC RDTE DIV., US, AGARD CP 567, pp 30.1, 1994.

2. Radio Wave Propagation Modeling, Prediction and Assessment, AGARD-AG-326, Ed. by Juergen H. Richter, NOSC/OASD, US, NATO/AGARD Monograph No. 326, ISBN 92-835-0598-0, December 1990.

3. Richter, J.G., "Structure, variability and sensing of the coastal environment," NCCOSC RDTE DIV., US, AGARD CP 567, pp. 1.1, 1994.

4. Philbrick, C.R., D.B. Lysak, T.D. Stevens, P.A.T. Haris, and Y.-C. Rau, "Atmospheric measurements using the LAMP lidar during the LADIMAS campaign," 16th International Laser Radar Conference, NASA Publication 3158, 651-654, 1992.

5. Philbrick, C.R., "Raman lidar measurements of atmospheric properties," Proceeding of the SPIE Symposium on Atmospheric Propagation and Remote Sensing III, Vol 2222, 922-931, 1994.

6. Rogers, L.T., "Effects of spatial and temporal variability of atmospheric refractivity on the accuracy of propagation estimates," NCCOSC RDTE DIV., US, AGARD CP 567, pp. 31.1- 31.7, 1994.

7. Hitney, H.V., J.H. Richter, R A. Pappert, K.D. Anderson, and G.B. Baumgartner, Jr., "Tropospheric radio propagation assessment," Proc. IEEE, Vol. 73, No. 2, pp. 265-283, Feb. 1985.

8. Engineer's Refractive Effects Prediction System (EREPS), Tech. Doc. 2648, NCCOSC RDTE Div., US Navy/NRaD, San Diego, CA, US, May 1994.

9. Hitney, H.V., "Hybrid ray optics and parabolic equation methods for radar propagation modeling," in Radar 92, IEEE Conference Proceedings No. 365, pp. 58-61, 1992.

10. Helvey, R., and L.W. Eddington, "Refractive variability during VOCAR 23 Aug.- 03 Sep. 1993, NAWCWPNS, US, AGARD CP 567, pp. 32.1, 1994.

11. Rosenthal, J., R. Helvey, and P. Greiman, "Satellite inferences of elevated duct variability over the eastern pacific during VOCAR," NAWCWPNS, US, AGARD CP 567, pp. 33.1, 1994.

Table 1. Predicted propagation loss data using RPO and IREPS based on using lidar profiles of refractivity at Point Mugu for the San Clemente Island to Point Mugu path (132 km).

Date (1993)	Time (UT)	Frequency (MHz)	Free Space Path Loss (dB)	IREPS** Loss (dB>f.s.)	RPO Loss (dB>f.s.)	RPO Total Path Loss (dB)
8/26	1013	(U) 374.9	126.3	+3	+2.5	123.8
		(V) 143.1	117.9	-8	-13.2	131.1
8/27	1025	(U) "	126.3	+3	+10.2	116.1
		(V) "	117.9	-6	-7.8	125.7
8/28	0906	(U) "	126.3	+3	-19.1	145.4
		(V) "	117.9	-8	-26.7	144.6
8/29	0800	(U) "	126.3	-43*	-28.0	154.3
		(V) "	117.9	-41*	-33.2	151.1
8/31	0945	(U) "	126.3	-46*	-43.2	169.5
		(V) "	117.9	-43*	-45.7	163.6

*Tropospheric-scatter-limited per IREPS program only
** very approximate losses from IREPS program

Table 2. Propagation loss data for San Clemente Island to Point Mugu, with measured and RPO predicted values based on atmospheric measurements of lidar profiles at Point Mugu.

Date (1993)/ Time (UT)	VOCAR Frequency (MHz)	Free Space Path Loss (dB)	VOCAR Sig. Path Losses* (dB>f.s.)	RPO Loss (dB>f.s.)	dB Diff sig/ pred loss	RPO Total Path Loss (dB)	Obs. Total Path Loss (dB)
8/26 /1013	(U) 374.9	126.3	-2 +/-10 dB	+2.5	-5	123.8	128.3 +/-10 dB
	(V) 143.1	117.9	-21 +/-9	-13.2	-8	131.1	138.9 +/-9
8/27 /1025	(U) "	126.3	-.5 +/-9	+10.2	-11	116.1	126.8 +/-9
	(V) "	117.9	-17.5 +/-4.5	-7.8	-10.	125.7	135.4 +/-4.5
8/28 /0906	(U) "	126.3	-13.5 +/-6.5	-19.1	5.6	145.4	139.8 +/-6.5
	(V) "	117.9	-34 +/-6	-26.7	7.3	144.6	151.9 +/-6
8/29 /0800	(U) "	126.3	-23 +/-6	-28.0	5	154.3	159.8 +/-6
	(V) "	117.9	-37 +/-6	-33.2	-4	151.1	154.9 +/-6
8/31 /0905	(U) "	126.3	-33.5 +/-4.5	-43.2	9.7	169.5	159.8 +/-4.5
	(V) "	117.9	-43 +/-7	-45.7	2.7	163.6	160.9 +/-7
			Overall	Avg. diff	-.74	dB	

* approx. 6 hour median and extremes (+/- 3 hours of 15min. samples about Lidar collection interval)

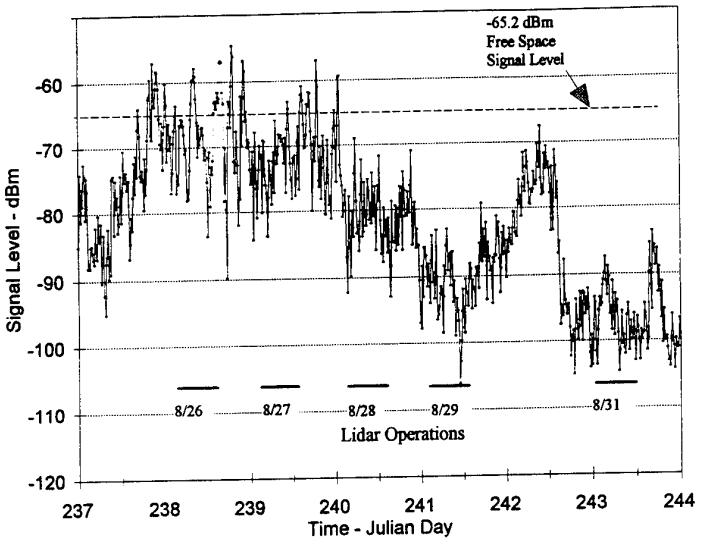

Figure 1. VOCAR received signal level at UHF for San Clemente Island to Point Mugu path (132 km) showing variability over an 8 day period, 15 minute samples.

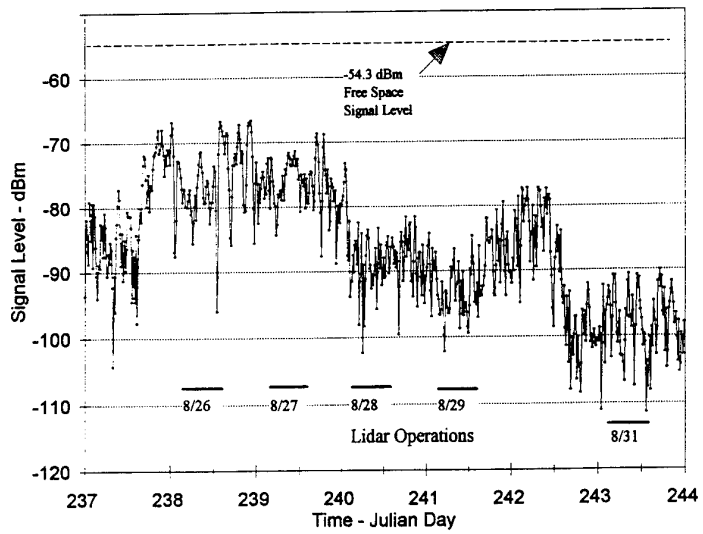

Figure 2. VOCAR received signal level at VHF for San Clemente Island to Point Mugu path (132 km) showing variability over an 8 day period, 15 min samples.

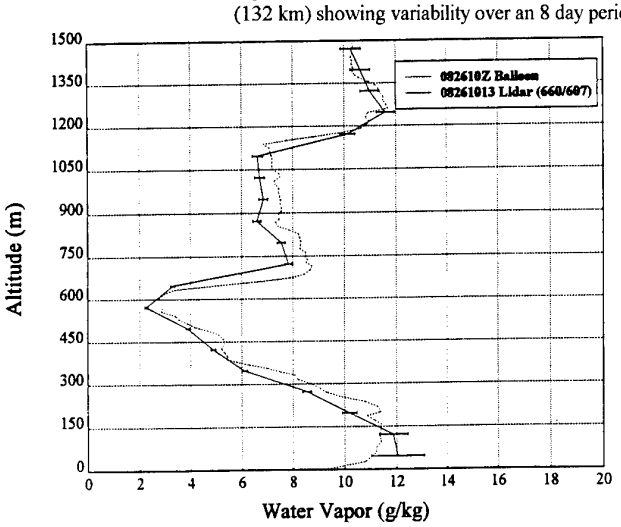

Figure 3. Example of lidar water vapor profile on 26 August 1993.

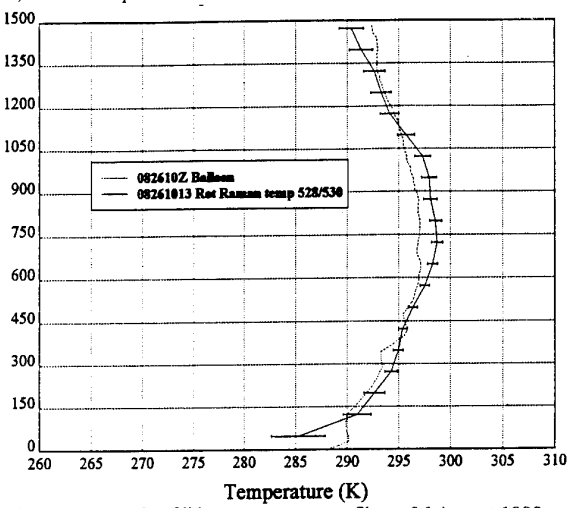

Figure 4. Example of lidar temperature profile on 26 August 1993.

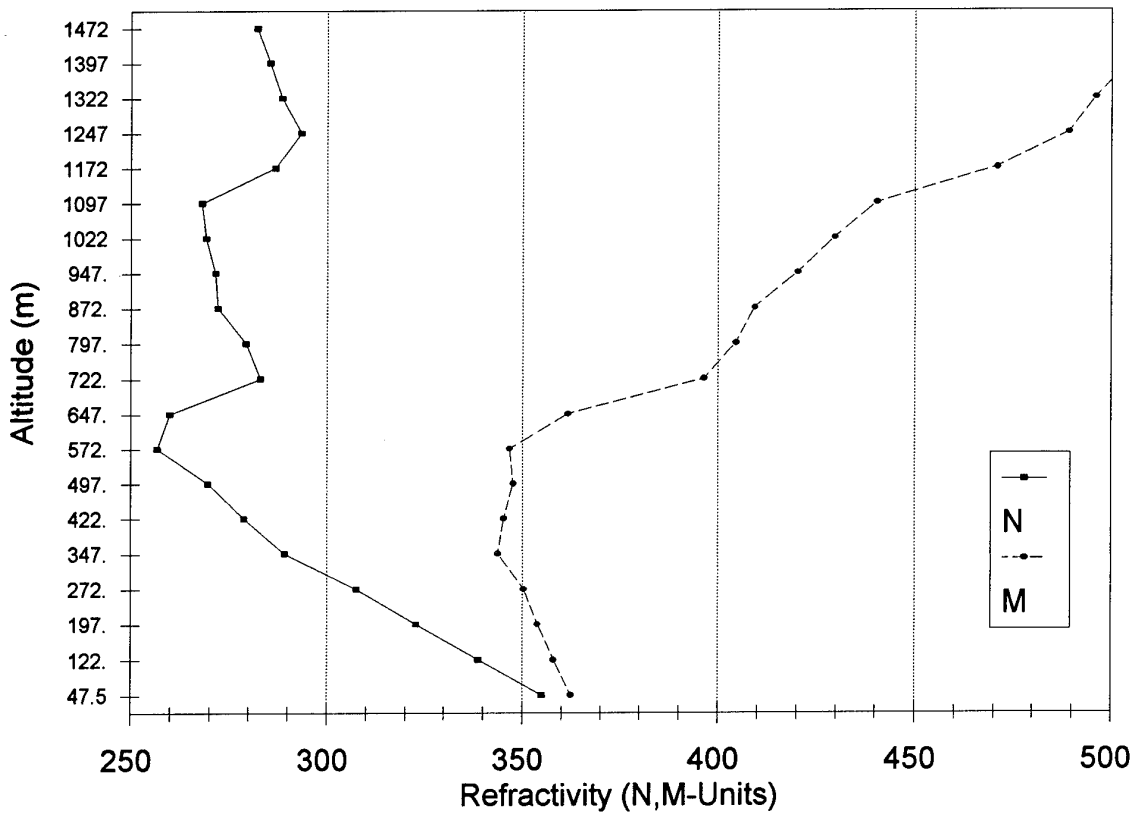

Figure 5. Refractive profiles on 26 August 1993 (1013Z) at Point Mugu showing a surface based duct to 600 m.

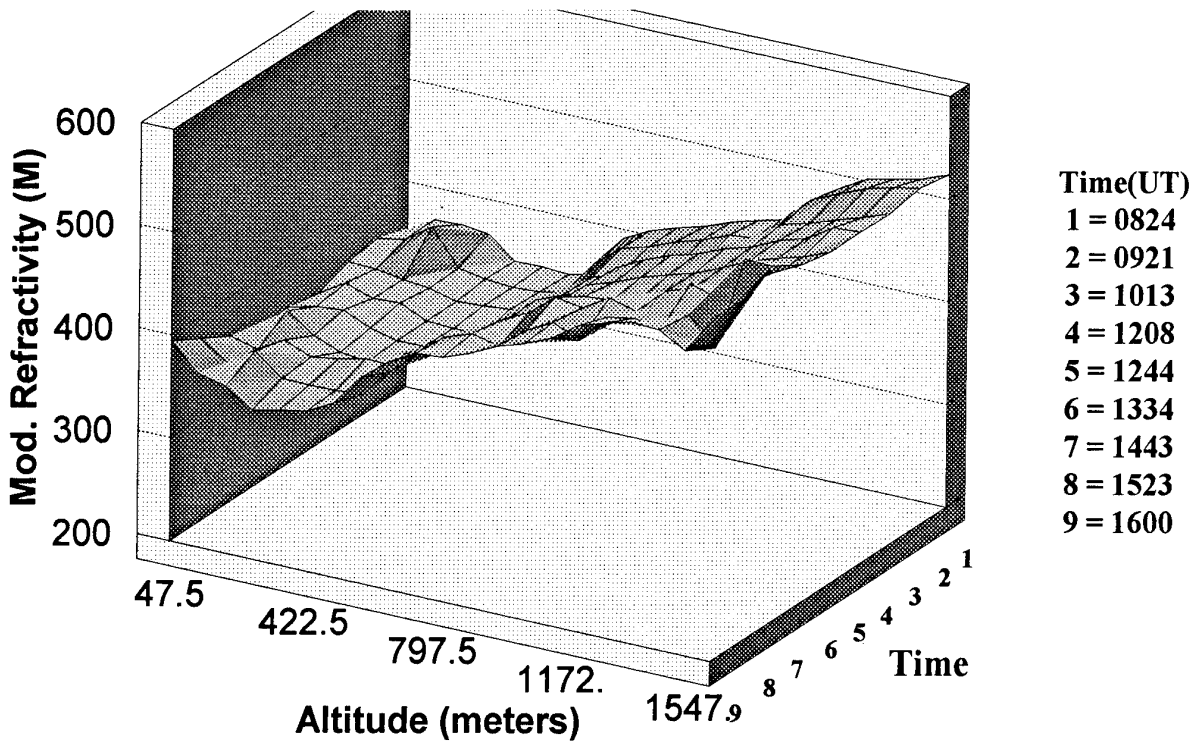

Figure 6. Surface contour of modified refractivity from lidar data on 26 August 1993.

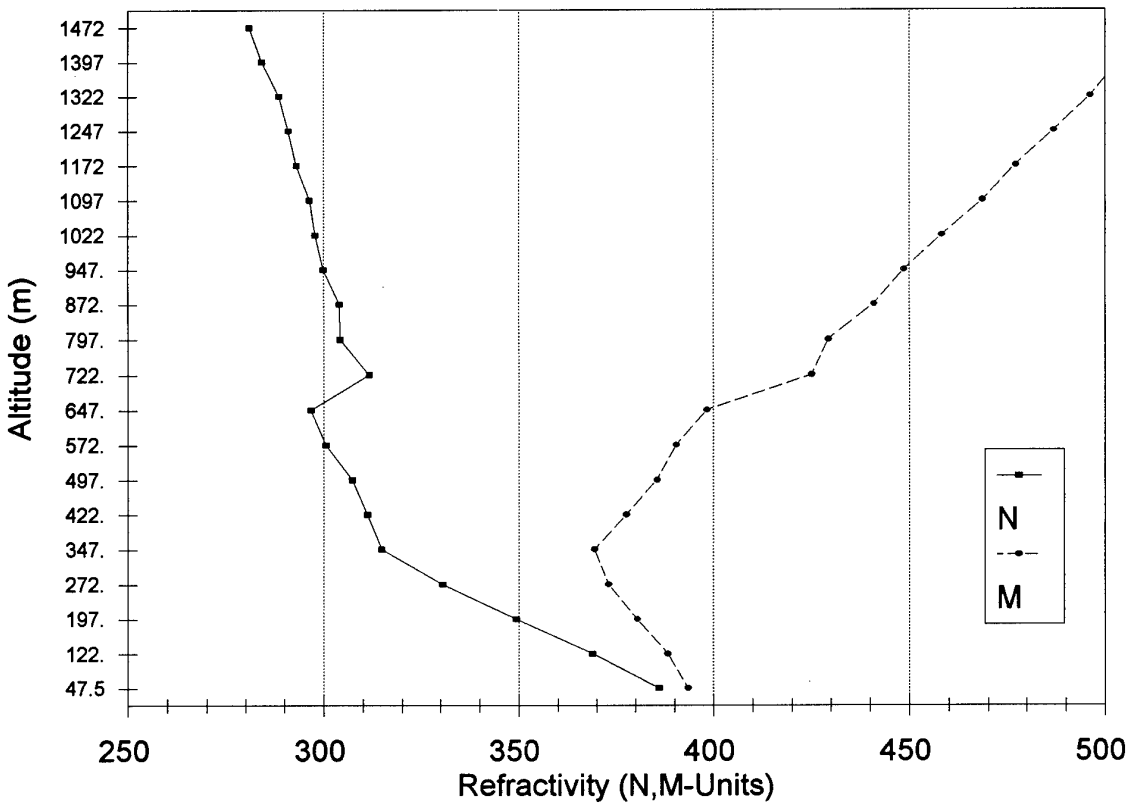

Figure 7. Refractive profiles on 27 August 1993 (1025Z) at Point Mugu showing a surface based duct to 350 m.

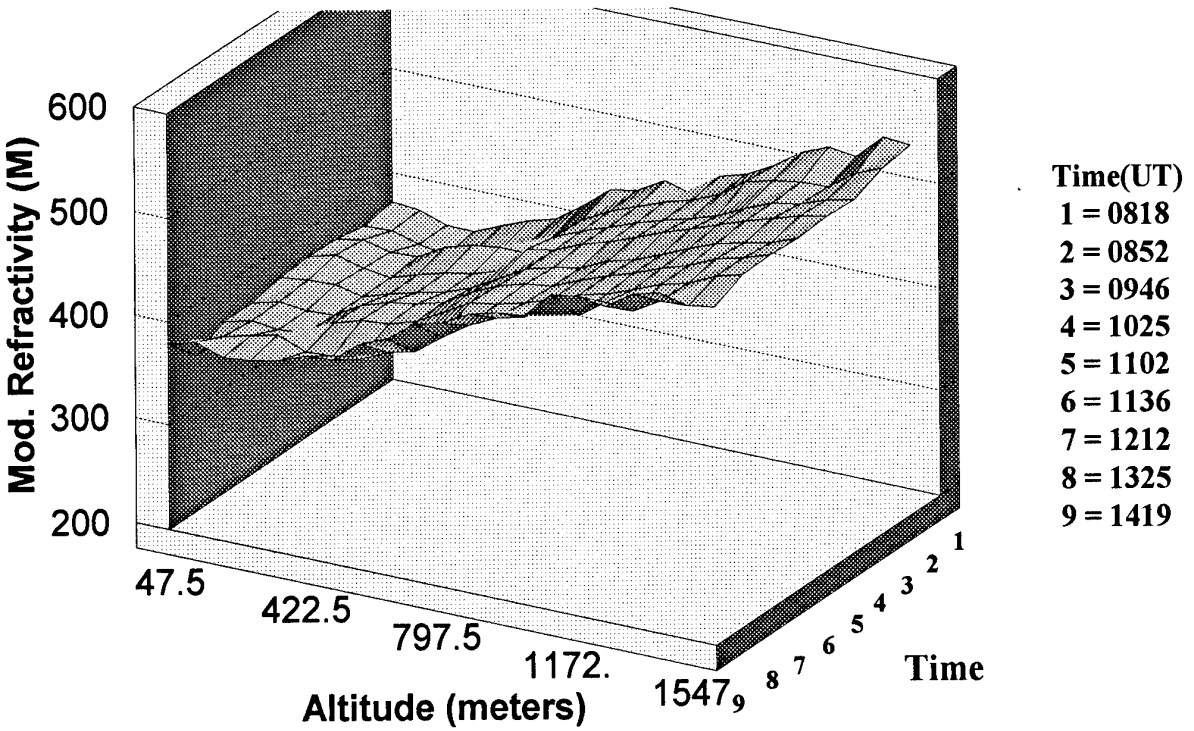

Figure 8. Surface contour of modified refractivity from lidar data on 27 August 1993.

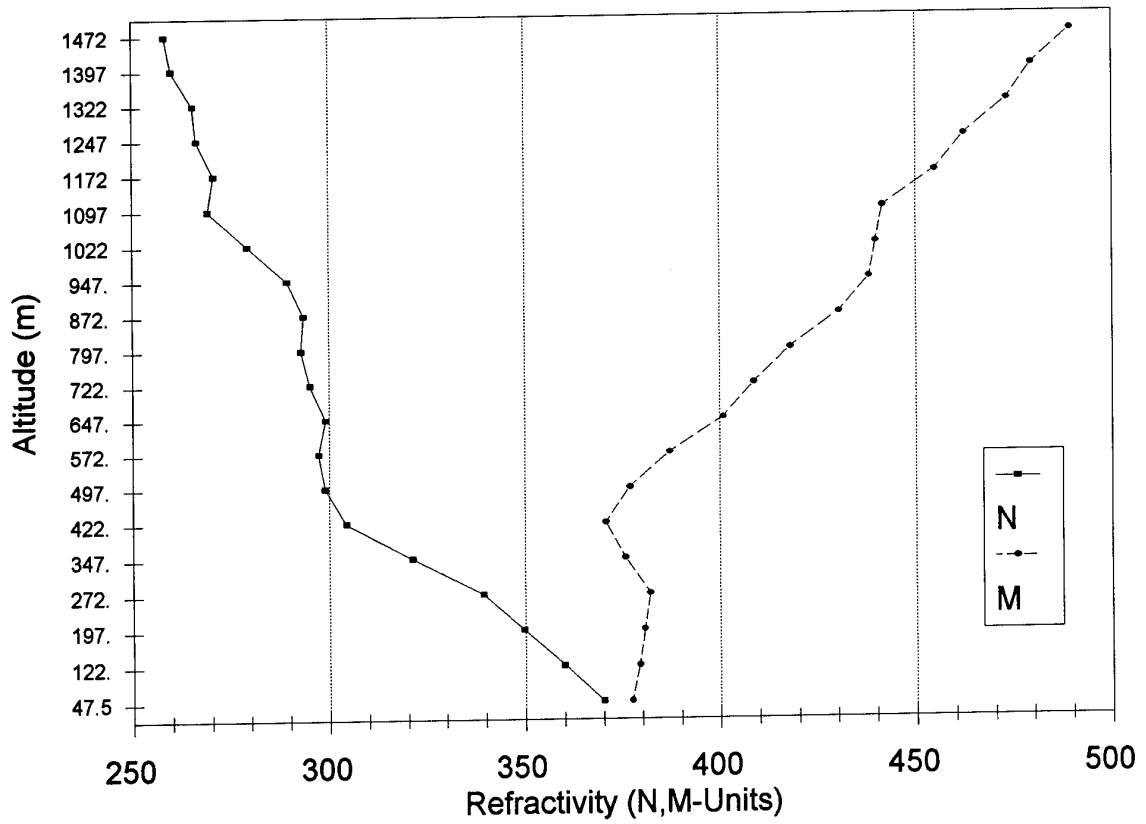

Figure 9. Refractive profiles on 28 August 1993 (0906Z) at Point Mugu showing a surface-based elevated duct at 425 m.

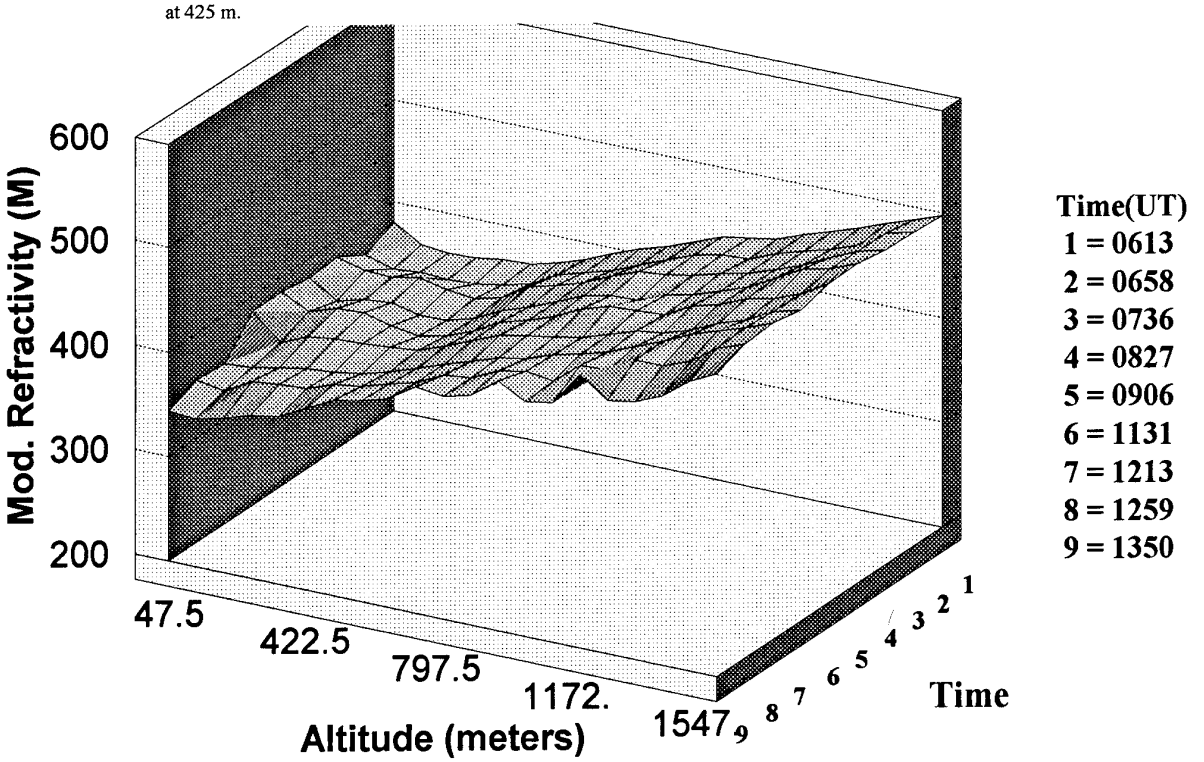

Figure 10. Surface contour of modified refractivity from lidar data on 28 August 1993.

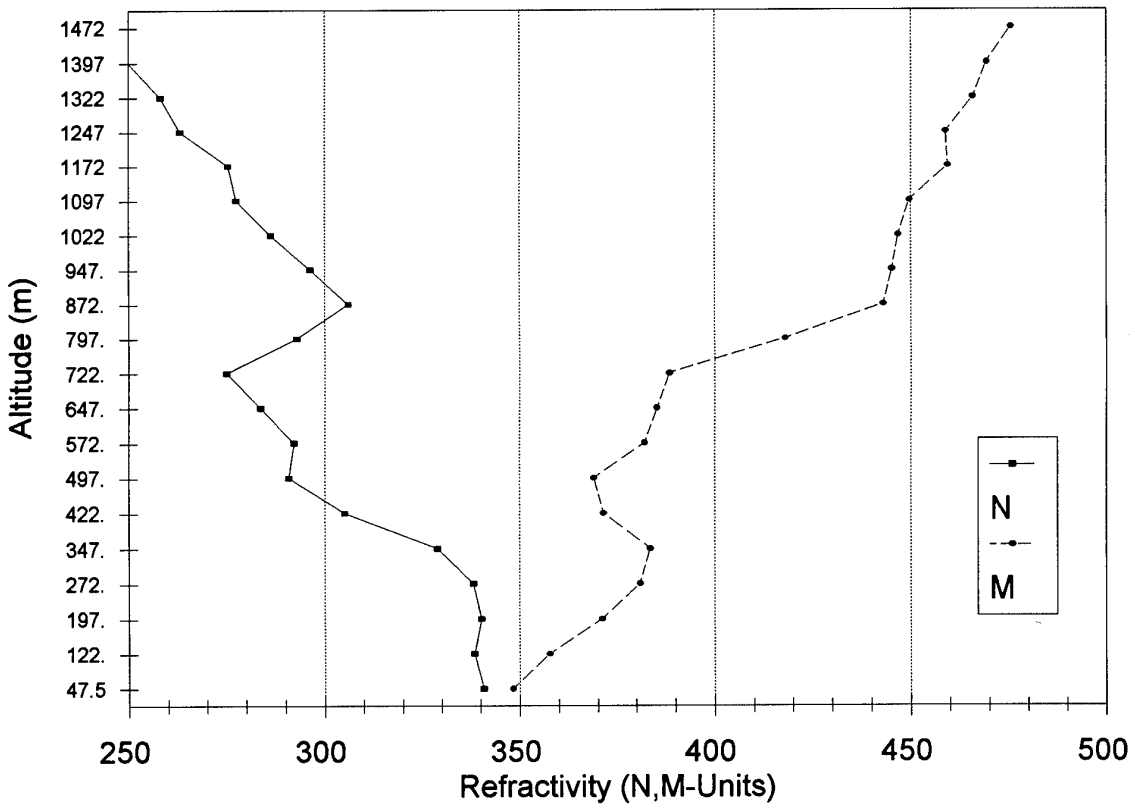

Figure 11. Refractive profiles on 29 August 1993 (0800Z) at Point Mugu showing an elevated duct 350-500 m.

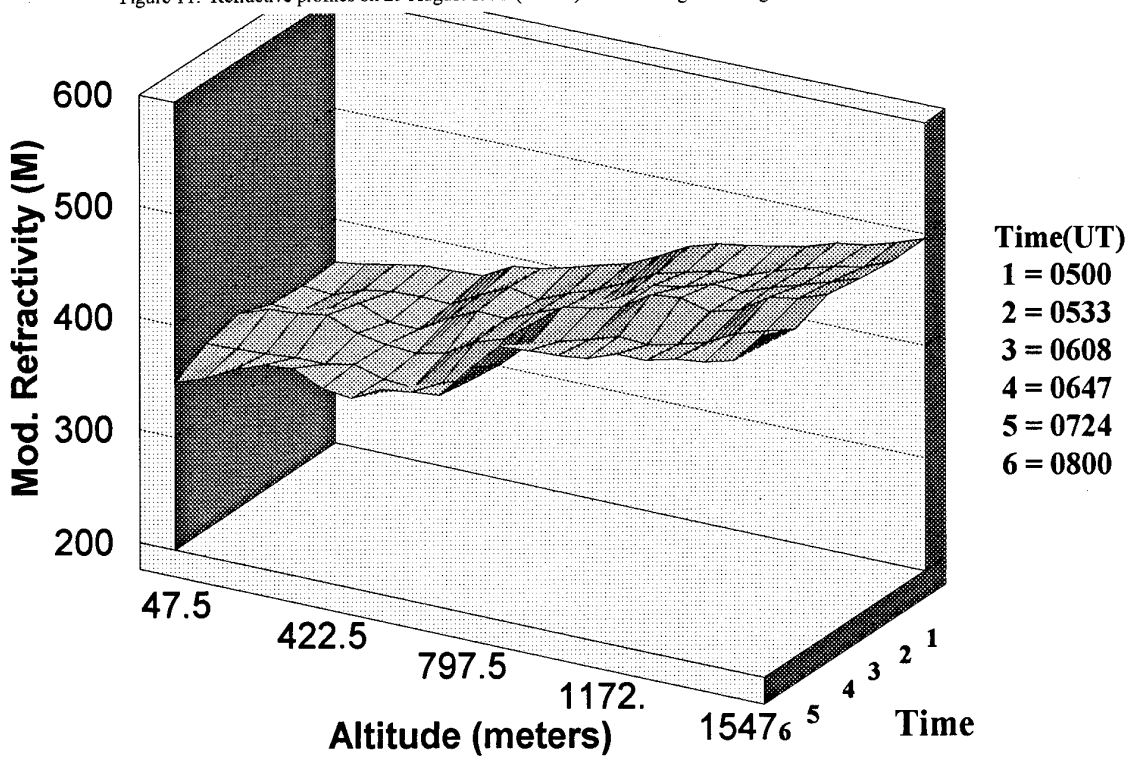

Figure 12. Surface contour of modified refractivity from lidar data on 29 August 1993.

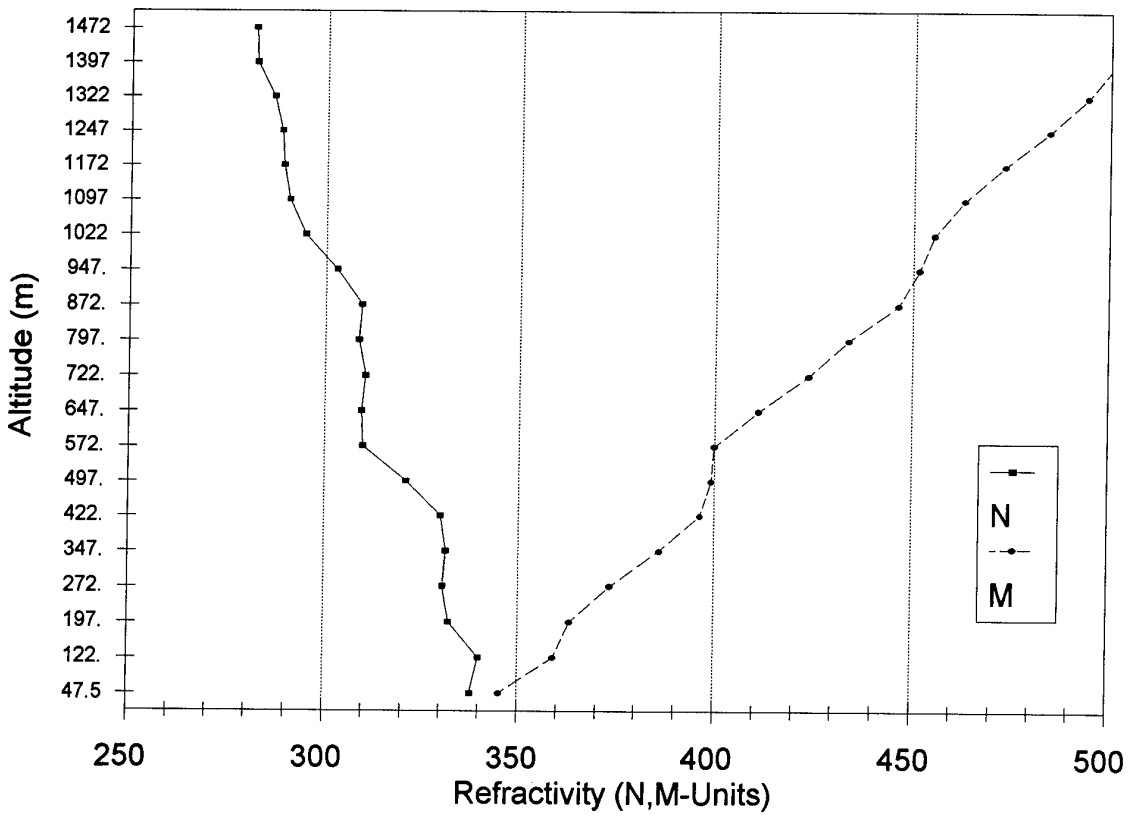

Figure 13. Refractive profiles on 31 August 1993 (0945Z) at Point Mugu showing non-anomalous conditions.

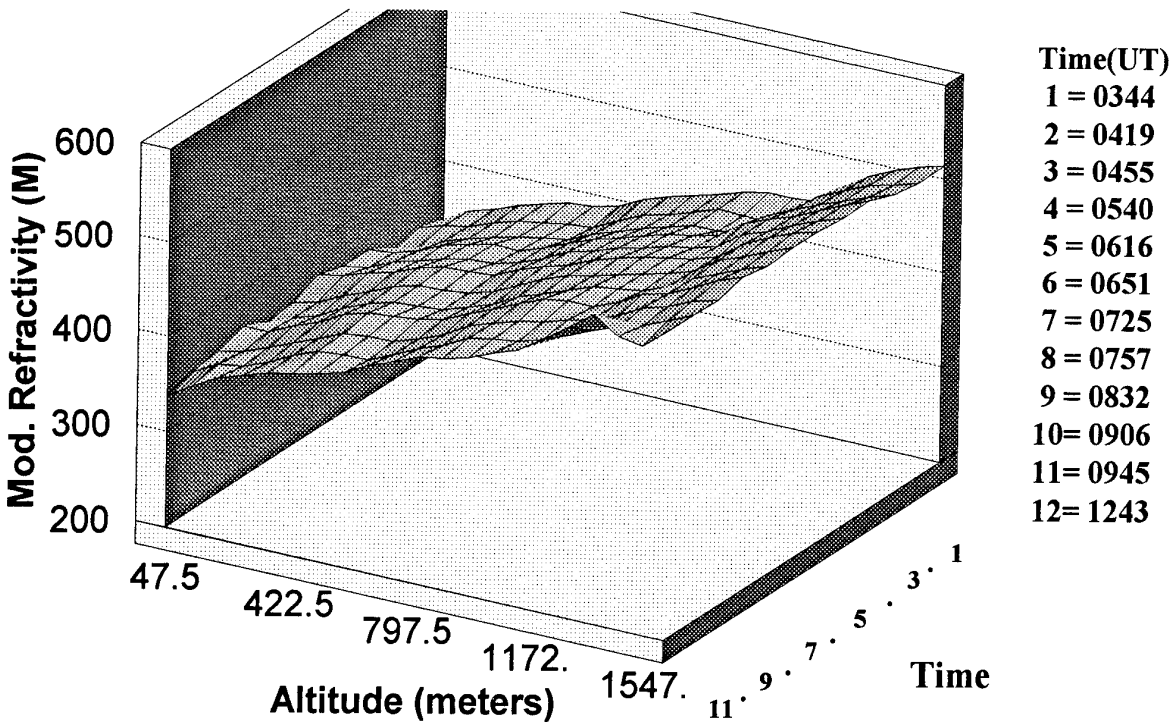

Figure 14. Surface contour of modified refractivity from lidar data on 31 August 1993.

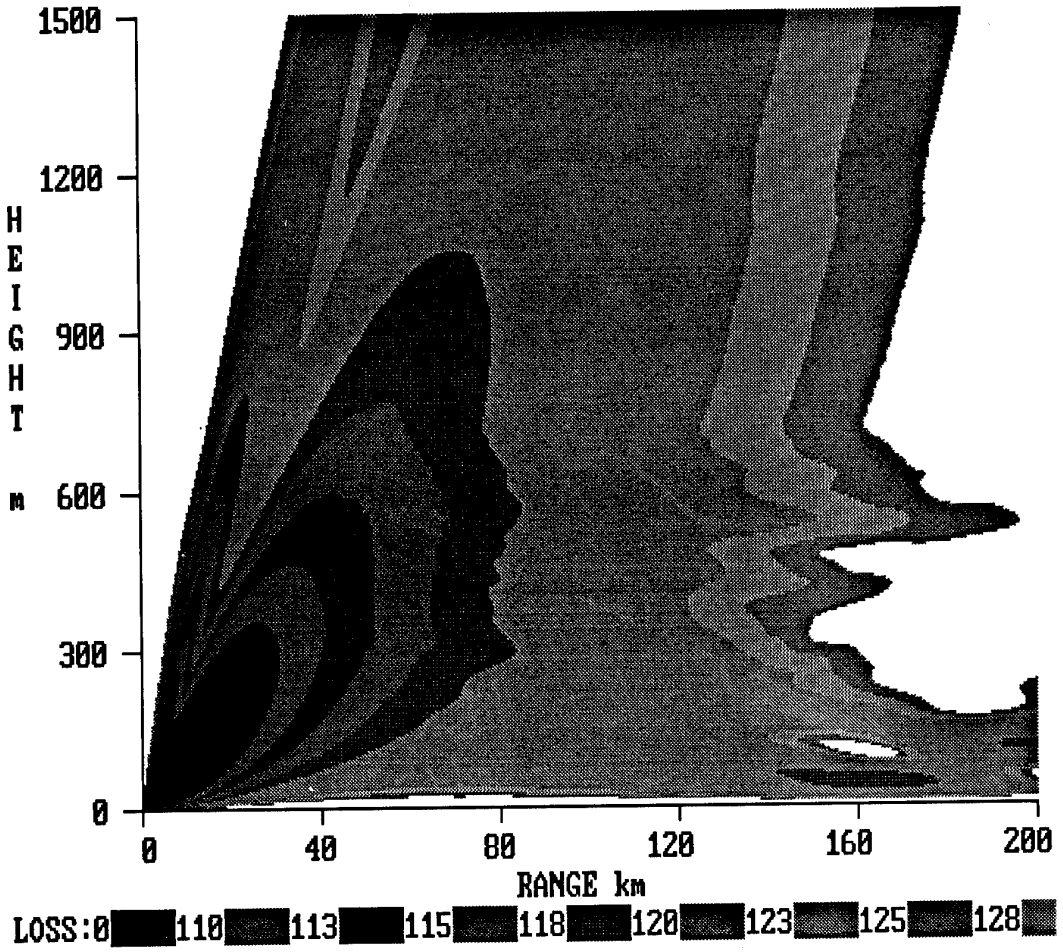

Figure 15. An example of propagation loss coverage calculated from RPO at UHF (374.9 MHz) based on lidar profiles at 1013Z on 26 August 1993.

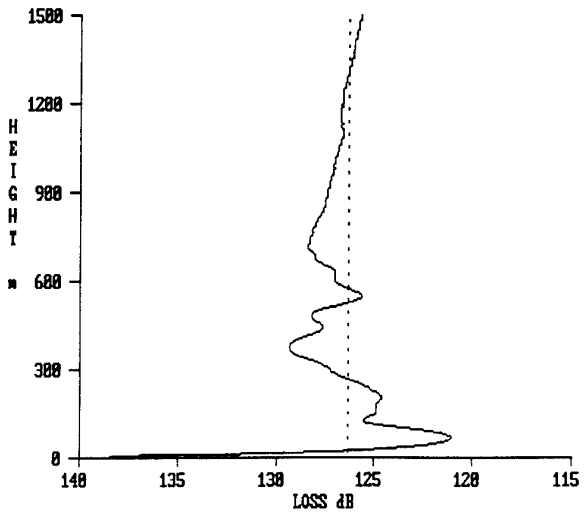

Figure 16. Calculation from RPO of UHF signal loss versus height relative to free space loss (for fixed antenna at 30.5 m) for conditions at 1013Z on 26 August 1993.

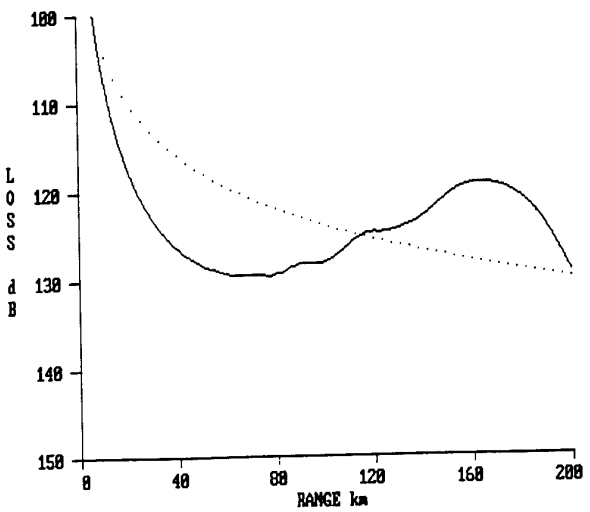

Figure 17. Calculation from RPO of UHF signal loss versus range at 30.5 m height relative to free space loss (dotted) for conditions at 1013Z on 26 August 1993.

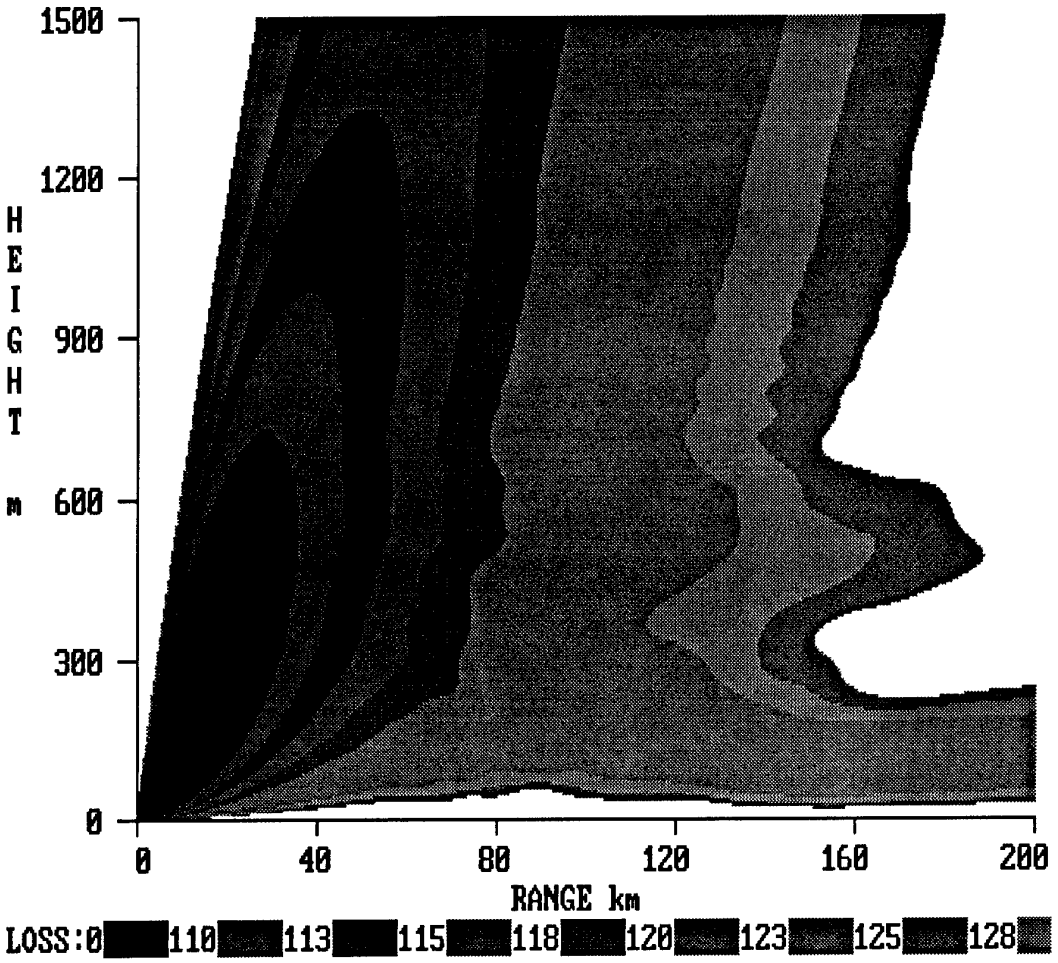

Figure 18. An example of propagation loss coverage calculated from RPO at VHF (143.1 MHz) based on lidar profiles at 1013Z on 26 August 1993.

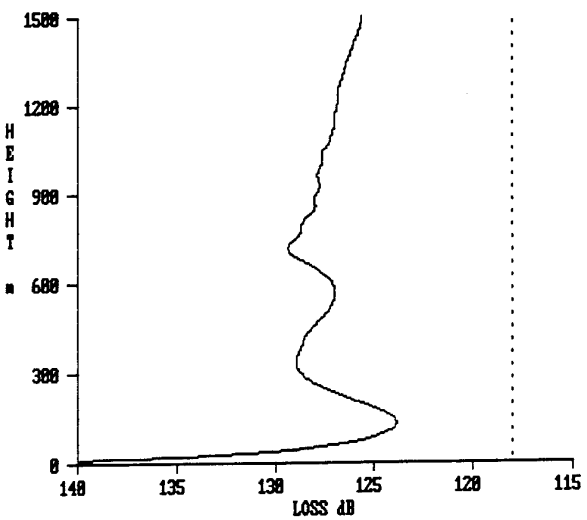

Figure 19. Calculation from RPO of VHF signal loss versus height relative to free space loss (for fixed antenna at 30.5 m) for conditions at 1013Z on 26 August 1993.

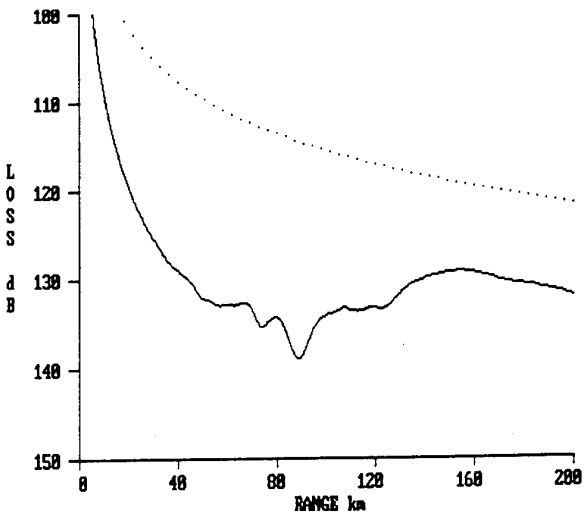

Figure 20. Calculation from RPO of VHF signal loss versus range at 30.5 m height relative to free space loss (dotted) for conditions at 1013Z on 26 August 1993.

DISCUSSION

K.H. CRAIG
How effective is the Raman lidar technique at tracking sharp temperature gradients? The same types of ducting layers over land can be caused by temperature inversions without significant water vapor effects.

AUTHOR'S REPLY
The rotational Raman technique provides an accurate way of measuring the temperature in narrow layers along the profile. At present we are limited to 75 m resolution elements, but should be able to measure the temperature gradients which are thicker than 75 meters.

J. ROSENTHAL
Regarding Dr. Craig's question concerning abilities of the lidar to detect temperature variations, it is common in coastal environments to have strong vertical moisture variations whenever a strong temperature inversion is present; this makes it more difficult to isolate the temperature sensitivity. However, the lidar is capable of detecting just the temperature variations.

AUTHOR'S REPLY
Yes, our present data set does not really contain strong temperature gradients, but we should be able to measure them adequately.